TECHNISCHE UNIVERSITÄT WIEN
Vienna | Austria

DIPLOMARBEIT

Bimetallische Nanocluster als Katalysatoren für selektive Hydrierungsreaktionen

Ausgeführt am

Institut für Materialchemie

der Technischen Universität Wien

unter der Anleitung von

Assistant Prof. Dr.in Noelia Barrabés Rabanal

Durch

Sebastian Mößlacher, BSc.

September 2025, Wien

TECHNISCHE UNIVERSITÄT WIEN
Vienna | Austria

MASTERTHESIS

Bimetallic nanoclusters as catalysts for selective hydrogenation reactions

Conducted at

Institute of materialchemistry

of TU Wien

under the supervision of

Assistant Prof. Dr.in Noelia Barrabés Rabanal

by

Sebastian Mößlacher, BSc.

September 2025, Vienna

Eidesstattliche Erklärung

Ich erkläre hiermit an Eides statt, dass ich die vorliegende Diplomarbeit selbstständig und ohne fremde Hilfe verfasst, andere als die angegebenen Quellen und Hilfsmittel nicht benutzt und die den benutzten Quellen wörtlich und inhaltlich entnommenen Stellen als solche erkenntlich gemacht habe.

Statutory Declaration

I declare that I have authored this thesis independently, that I have not used other than the declared sources / resources, and that I have explicitly marked all material which has been quoted either literally or by content from the used sources.

Acknowledgement

Most importantly, a big thank you to my supervisor Noelia Barrabés, for her continued support during my work on this thesis, the side quests and of course for the opportunity of my research stay. To not only work on something, but to also be allowed to experiment and learn new things in the laboratory is something very appreciated from my side. Additionally, Prof. Yuichi Negishi has earned my biggest gratitude for not only providing my master studies with such well-designed nanoclusters, but also to opportunity to learn and experience the Japanese chemical world.

Working in the laboratory was made way more enjoyable due to the presence of all our ClusCat Team members as well as the knowledge and experience of the Sanchez Sanchez Team.

Zusammenfassung

Der Übergang zu erneuerbaren Energien hat Wasserstoff als Vorreiter für vielversprechende alternativen zu herkömmlichen fossilen Brennstoffen gebracht. Grüne Wasserstoffproduktion, im speziellen die Herstellung via der Wassergas Shift (WGS) Reaktion, verlangt hoch effiziente Katalysatoren. Für die Entwicklung solcher Katalysatoren ist ein hohes Verständnis bezüglich dem Reaktionsmechanismus und den Einflüssen der Komponenten des Katalysators auf atomarer Ebene von Nöten.

Diese Arbeit untersucht die Einflüsse von Variationen an Ligandensphären auf bimetallischen $PtAu_{24}$ Nanoclustern und deren Interaktionen mit dem Zeroxid Supportmaterial um die Basis an Nanoclusterkatalyse in seinen Grundschritten voran zu treiben. Um die genauestens charakterisierten $PtAu_{24}$ Kerne zu modifizieren wurden Ligandenaustausch Reaktionen durchgeführt, dies führte zu singulären sowie gemischten Liganden Konfigurationen an der Clusterhülle. Die Synthese, sowie die initiale Charakterisierung der Nanocluster wurde von dem Negishi Labor durchgeführt. Anschließend wurden diese auf das Supportmaterial Zeroxid (CeO_2) aufgetragen und via der CO Oxidationsreaktion und der Wassergas shift Reaktion getestet.

Oberflächen- und Strukturänderungen, inklusive Ligandenmigrationen während der thermischen Konditionierung und Reaktion wurden mit Diffuse Reflectance Fourier Transform Spectroscopy (DRIFTS) und X-ray Absorption Fine Structure (XAFS) analysiert. Die kinetischen Versuche zeigten, dass die Ligandenzusammensetzung einen ausschlaggebenden Einfluss auf die katalytische Aktivität und die Stabilität haben. Gewisse ligandenumhüllte Cluster demonstrierten hohe Aktivitäten bei schon geringen Temperaturen, während andere hervorragenden Stabilität beim mehrmaligen Zyklieren von Reaktionen. Thermisches Pretreatment zeigte starke Einflüsse auf die Effizienz der Umwandlung and Produkt und Langzeitstabilität, was eine Art Balanceakt zwischen Aktivität und Stabilität bei ligandenumhüllten Systemen demonstriert.

Spektroskopische und strukturelle Analysen zeigten, dass Ligandenvariation zu eindeutig unterschiedlichen Strukturevolutionen führt. Dies trug einen Einfluss auf die Carbonat und Format Intermediat Formation mit sich, welche in spezifischen Temperaturfenstern ersichtlich war. Diese Ergebnisse offenbarten mechanistische Einblicke in ligandenabhängige Katalyse was Designoptionen für maßgeschneiderte Nanocluster Katalyse im Hinblick auf effiziente und stabile Wasserstoff Produktion in erneuerbarer Trebstofftechnologie präsentiert.

Abstract

The transition toward sustainable energy solutions has brought hydrogen to the forefront as a promising alternative to conventional fossil fuels. Green hydrogen production, particularly via the water–gas shift (WGS) reaction, demands highly efficient catalysts. Designing such catalysts requires a deep understanding of both the reaction mechanism and the atomic-level contributions of catalyst components.

This study investigates the influence of ligand shell variation on bimetallic $PtAu_{24}$ nanoclusters and their interaction with a CeO_2 support, aiming to elucidate key factors governing nanocluster catalysis. Ligand exchange reactions were used to modify a well-characterized $PtAu_{24}$ core, producing both single- and mixed-ligand configurations. These nanoclusters, synthesized by the Negishi Laboratory, were supported on CeO_2 and evaluated for CO oxidation and WGS reactions.

Surface and structural changes, including ligand migration during thermal conditioning and reaction, were probed using Diffuse Reflectance Infrared Fourier Transform Spectroscopy (DRIFTS) and X-ray Absorption Fine Structure (XAFS) analysis. Kinetic measurements revealed that ligand composition substantially affects both catalytic activity and stability. Certain ligand-protected clusters demonstrated high activity even at low temperatures, while others offered enhanced stability over repeated reaction cycles. Thermal pretreatment was found to strongly influence both conversion efficiency and long-term durability, highlighting a trade-off between activity and stability in ligand-protected systems.

Spectroscopic and structural analyses showed that ligand variations lead to distinct structural evolution patterns, affecting the formation of carbonate and formate intermediates, which occurred only within specific temperature windows. These findings provide mechanistic insight into ligand-dependent catalytic behavior and offer design principles for tailoring nanocluster catalysts toward efficient and stable hydrogen production in sustainable fuel technologies.

Table of Contents

1 Introduction

Hydrogen generation from the water-gas shift (WGS) reaction stands at the forefront of clean energy technologies, making catalysis—and particularly heterogeneous catalysis—crucial for realizing efficient conversion processes. The WGS reaction, which transforms carbon monoxide and water vapor into hydrogen and carbon dioxide, relies fundamentally on finely tuned catalysts to achieve high activity and selectivity under practical conditions.

Catalysis, at its core, refers to the acceleration of chemical reactions by substances (catalysts) that remain unchanged after the process[1]. These substances facilitate conversion paths that lower activation energy, increase reaction rates, and improve product selectivity without themselves being consumed.[2] The effectiveness of a catalyst is shaped by several factors, including temperature, pressure, structure, and composition. Heterogeneous catalysis involves reactants and catalysts in different phases—most often, gases interacting with solid catalysts—ensuring that reactions occur at active sites on the catalyst's surface. [3–5] Here, the interplay between geometric structure, electronic configuration, and binding energies determines both the efficiency and outcome of the process. [5,6]

Recent advances in atomic-level characterization have revealed fundamental limitations of conventional bulk or nanoparticulate catalysts. These limitations include broad size distributions, poorly defined structures, and difficulty in correlating atomic arrangement with catalytic behavior. Addressing these challenges, atomically precise metal nanoclusters (NCs) have emerged as a powerful platform. With fully resolved atomic structures, narrow size distributions, and well-defined ligand environments, metal NCs allow for the establishment of direct structure–property relationships. Their atomically precise nature makes it possible to systematically study the influence of cluster size, elemental doping, or ligand modification on catalytic performance.[7,8]

1.1 Nanoclusters: atomically precise catalysts active sites

Nanoclusters, typically defined as metal aggregates with dimensions below 2 nm and fewer than ~100 atoms, occupy a critical size regime between molecular complexes and bulk nanoparticles.

In this domain, size- and composition-dependent properties become prominent. Compared to bulk metals or larger nanoparticles, nanoclusters exhibit distinct surface-to-volume ratios, discrete energy levels, and unique quantum-size effects[9,10]. In these ultra-small systems, orbital overlap between metal atoms leads to delocalized electronic states. As the cluster size increases, the density of electronic states gradually approaches that of bulk metals, shrinking the HOMO–LUMO bandgap until the distinction becomes negligible. This size-dependent evolution of electronic structure underpins the unusual reactivity of nanoclusters and highlights the importance of synthetic control in their preparation[9–11].

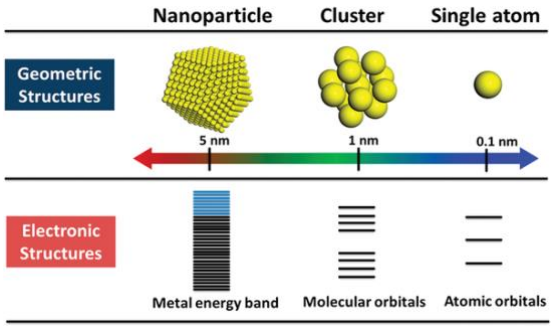

Figure 1: dependence of electronical structure of size[11]

Achieving structural homogeneity requires careful stabilization during synthesis, typically through the use of organic ligands. Ligands not only prevent aggregation and preserve atomic precision, but also actively influence the nanocluster's electronic structure and reactivity. Among various ligand classes—thiols, alkynes, carbenes, and others—thiolates are particularly versatile. Sulfur–metal interactions impart remarkable stability, enable fine-tuned surface chemistry, and allow for functionalization strategies that expand catalytic applications. At the same time, ligands exhibit a dual role: while they can enhance selectivity or promote specific reactions (e.g., semi-hydrogenations), they may also block active sites or hinder reactivity in others (e.g., alcohol oxidation)[9,10,12]. The delicate balance between stabilization and reactivity remains a central theme in nanocluster catalysis.

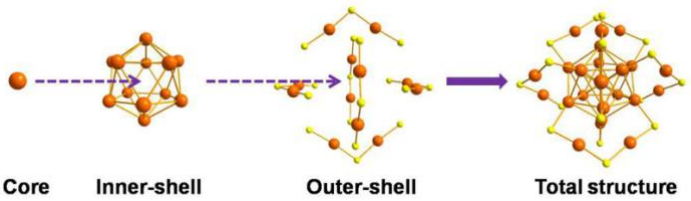

Figure 2: schematic core and staple unit structure of Au_{25} nanocluster[13]

Within this context, gold nanoclusters protected by thiolate ligands [$Au_m(SR)_n$] represent one of the most extensively studied systems. Their thermodynamic stability is often restricted to specific compositions, reflecting strong electronic shell closing effects and geometric preferences[11]. A prototypical example is the $Au_{25}(SR)_{18}$ nanocluster, which possesses a precisely defined structure: a 13-atom icosahedral Au core, with a central atom surrounded by 12 surface atoms, further stabilized by six staple-like motifs (-S–Au–S–Au–S-) that connect 18 thiolate ligands. This molecularly precise entity displays D_2h symmetry and serves as a model catalyst in fundamental and applied studies[12,14,15]. Notably, Au nanoclusters provide a unique testing ground to investigate how metal–ligand interactions, quantum confinement, and structural stability collectively shape catalytic behavior.

The present thesis focuses on understanding the catalytic properties of thiol-protected metal nanoclusters, with particular emphasis on gold nanoclusters. By exploring the interplay between cluster size, ligand environment, and reaction type, this work aims to shed light on fundamental principles governing nanocluster catalysis. In doing so, it seeks to establish how atomic precision can be translated into tailored catalytic performance, thereby bridging the gap between molecular catalysis and traditional nanoparticle-based heterogeneous catalysis.

1.1.1 Doping Effects

A powerful strategy to tune the catalytic properties of atomically precise gold nanoclusters is heteroatom doping, i.e., substituting one or more gold atoms with foreign metals. Doping alters the nanocluster's electronic structure, geometric configuration, and thermodynamic stability, thereby modulating its catalytic activity. Introducing single atoms into the nanocluster framework can perturb the energy levels, shift the HOMO–LUMO gap, tune charge distribution, and in some cases endow the system with entirely new reaction pathways[9,11,16].

Typical dopants studied to date include transition metals such as Pt, Pd, and Cu, which exhibit distinct site preferences and thereby induce unique structural and catalytic consequences. Experimental and computational investigations have shown that Cu atoms preferentially occupy staple positions (Au–S–Au motifs in the ligand shell), where they can stabilize the Au–thiolate framework and influence the charge distribution at the cluster surface[7]. In contrast, Pt and Pd

atoms preferentially occupy the central position of the icosahedral Au_{13} core, giving rise to $M_1Au_{24}(SR)_{18}$ compositions (M = Pt, Pd)[7,8,11,12]. This endohedral substitution enhances stability while simultaneously creating electronic perturbations that often increase the catalytic activity in reactions such as CO oxidation and hydrogenation[7,8].

The ability to substitute gold atoms at specific positions lends a remarkable level of control over catalytic design, but it also highlights inherent challenges. In practice, not all atomic positions within a cluster can be doped arbitrarily, as the site preference of different dopants depends on their size, electronegativity, and affinity toward sulfur ligands[7,8]. Furthermore, while isolated doping has been systematically studied, the behavior of multi-doped systems—where more than one foreign atom is introduced—remains less understood. Questions about synergistic effects, cooperative behavior between dopants, and the resulting impact on catalytic selectivity and reaction mechanisms remain open. Addressing these challenges is essential for translating doping strategies into predictive design principles for cluster-based catalysis.

1.1.2 Support and Ligand Effects

Another crucial factor in determining the catalytic performance of thiolated gold nanoclusters is the interaction with support materials and ligands. In heterogeneous catalysis, cluster immobilization on supports not only prevents aggregation but also modifies cluster stability, electronic properties, and reaction pathways. Depending on the nature of the support, the same gold nanocluster can exhibit very different catalytic performances, underlying the importance of cluster–support synergy[7,12,16,17].

Support materials are often classified into two broad categories:

- Reactive/reducible supports, such as CeO_2 and TiO_2, which engage in strong interactions with the clusters, can transfer charge, and often provide active sites at the cluster–support interface[18,19].
- Inert/non-reducible supports, such as Al_2O_3 or SiO_2, which primarily serve a stabilizing role without significantly altering the cluster's electronic structure[18,20].

Among these, reducible metal oxides such as ceria (CeO_2) have attracted particular attention. Owing to its ability to generate surface oxygen vacancies and mediate oxygen storage/release, CeO_2 promotes reactions such as low-temperature CO oxidation. Studies comparing Au25 on CeO_2 versus TiO_2 highlight the enhanced low-temperature activity of the ceria-supported system, which has been attributed to more efficient electron transfer, altered charge distribution, and water activation at oxygen vacancy sites. At the Au–CeO_2 interface, adsorbed CO and activated H_2O cooperate in reaction pathways that are inaccessible to unsupported clusters[7,8,16,17,19].

Beyond the support, organic ligands also play a dual and sometimes contradictory role. On one hand, thiolates (–SR), alkynes, or carbenes stabilize the clusters against coalescence, ensuring atomic precision throughout the reaction. On the other hand, ligands can partially block surface sites, restricting access for reactants and thereby decreasing catalytic activity[12,14,15]. The challenge lies in balancing these effects: while removal or partial modification of ligands can unlock activity by opening catalytic sites, carefully chosen ligands can also tune selectivity by steering adsorption and activation processes toward specific intermediates.

1.1.3 Pretreatment Effects and Ligand Dynamics

A defining feature of thiolated gold nanoclusters is their organic ligand shell, which provides stability against aggregation but simultaneously passivates active sites and hinders reactant access to the metal core. Consequently, pretreatment strategies—aimed at modifying or partially removing ligands—play a decisive role in activating nanoclusters for catalysis[7,8,17]. The extent and method of pretreatment strongly affect catalytic performance, structural stability, and the ultimate nature of the active site.

Early studies demonstrated that as-synthesized, ligand-protected clusters are often catalytically inactive, as bulky ligands impede reactant adsorption. For example, Yin[21,22] et al. observed that untreated $Au_{25}(SR)_{18}$ clusters exhibit negligible CO adsorption, underscoring the importance of surface cleaning prior to catalytic testing. Controlled pretreatment, typically involving oxidative atmospheres (O_2, O_3, or air) or thermal annealing, facilitates thiolate desorption, removes organic residues from synthesis, and exposes otherwise inaccessible active sites. However, there is no consensus in the field regarding the optimum degree of ligand removal. While many studies affirm that at least partial desorption is required for activity enhancement, other reports suggest

that larger clusters may remain catalytically active even with significant ligand coverage. For Au_{25} clusters specifically, the unique staple motif structure makes ligand removal particularly consequential, as excessive desorption can destabilize or collapse the cluster framework[7,17,21,23].

Another layer of complexity arises from the competing requirements of pretreatment. On one hand, sufficient oxidative treatment is usually necessary to eliminate thiols and organic fragments; on the other hand, subsequent reductive pretreatment (e.g., H_2 atmosphere) is often employed to restore metallic states within the cluster core, which may otherwise oxidize during the cleaning process. The sequence, atmosphere, and temperature profile of such treatments therefore need to be carefully optimized to balance ligand removal, structural integrity, and maintenance of atomic precision. Indeed, the same nanocluster may show widely different activities depending on whether pretreatment was oxidative-only, reductive-only, or a combined treatment[7,17,21,23].

Previous research by Barrabés group provides clear insights, that thiolate ligands from gold nanoclusters migrate onto the CeO_2 support during deposition and oxidative pretreatment. This process results in the formation of oxidized sulfur species (such as disulfides, sulfites and sulfates) on CeO_2, which fundamentally alters the support's electronic and adsorption properties, as well as the accessibility of the gold clusters and their catalytic performance. Ligand migration and redistribution are now recognized as being fundamental for catalytic selectivity and activity, particularly in oxidation reactions[24].

Beyond simple ligand removal, pretreatment can also trigger ligand migration and metal redistribution phenomena, which profoundly alter catalytic behavior. For instance, in bimetallic doped systems such as $PtAu_{24}$ or $PdAu_{24}$, post-synthetic activation has revealed the migration of dopant atoms from the core to surface positions. This migration alters the geometry of staple motifs, redistributes charge across the nanocluster, and often enhances performance by bringing catalytically active dopants into direct contact with reactants at the surface[8,17,24,25].

The implications are significant: pretreatment is not merely a cleaning step, but a deterministic factor in defining the final structure–function relationship of cluster catalysts. Whether stability is preserved, whether dopant atoms migrate to the surface, and whether the ligand shell undergoes controlled desorption or catastrophic collapse—all these outcomes depend on how

pretreatment is engineered. Importantly, these transformations also reflect the influence of the support material, as oxide supports like CeO_2 can stabilize partially desorbed clusters, mediate charge transfer, and even participate in anchoring detached thiols or redistributed metal atoms, thereby reshaping the catalyst interface.

1.1.4 Structural Development of Nanocatalytic Systems Under Reaction

A comprehensive understanding of catalytic processes at the atomic level has positioned nanoclusters as a critical focus in catalysis research, with the overarching goal of uncovering fundamental mechanisms that govern activity and selectivity. Previous studies, including those from the Barrabés group[7,8,17,24–27], have demonstrated how atomically precise nanoclusters can drive highly selective transformations and how their unique tunability—through size, doping, ligation, or support effects—makes them a model platform for mechanistic investigation. These findings collectively highlight that detailed structural and electronic characterization is indispensable if one aims to establish a precise correlation between structure and catalytic performance.

Central to this effort has been the advancement of in situ and operando spectroscopic techniques, which allow researchers to probe catalysts during activation and under realistic reaction conditions, rather than relying solely on ex situ “frozen” snapshots. For thiol-protected gold nanoclusters, such methods are particularly powerful: their atomically resolved structures provide well-defined benchmarks, enabling even subtle changes to be unambiguously tracked at the single-atom scale. This makes it possible to disentangle processes that typically happen simultaneously in larger, less defined nanoparticles—such as ligand detachment, support interaction, dopant migration, and core restructuring[7,28,29].

X-ray absorption fine structure (XAFS) spectroscopy, for instance, has proven invaluable in mapping local structural evolution. It can monitor metal–metal and metal–sulfur coordination numbers, thereby detecting the stepwise removal of ligands, changes in cluster geometry, or even dissolution of the core. Time-resolved XAFS enables one to follow these transformations during heating, pretreatment, or catalytic turnover, thus bridging nanoscale structure with macroscopic reactivity[8,26,28].

Complementing this, infrared (IR) spectroscopy—especially when combined with probe molecules such as CO—offers a highly sensitive tool to investigate surface evolution. CO adsorption studies reveal the oxidation state and coordination environment of exposed metal atoms, while following shifts in vibrational frequencies provides insight into electron back-donation between the metal surface and the adsorbate. These subtle variations directly report on changes in accessible active sites, ligand dynamics, and dopant redistribution. By coupling IR analysis with reaction monitoring, one can not only detect the onset of activity but also deduce the underlying mechanism, such as the formation of surface intermediates or the blocking effect of residual ligands[8,26,28].

The synergy of these techniques under operando conditions has been critical in disclosing phenomena such as:

- Ligand removal and partial retention, distinguishing between beneficial exposure of active sites versus destabilizing desorption[8,17,26,27].
- Metal atom migration and segregation, including the outward diffusion of Pt and Pd dopants from the Au core during activation[8].
- Support-induced restructuring, where reducible oxides like CeO_2 stabilize partially desorbed clusters and alter charge distribution at the interface[8,17,26,30].

What makes such insights possible is the combination of advanced spectroscopy with atomically precise catalysts: because the starting structure of systems like $Au_{25}(SR)_{18}$ is fully known, any modification—whether a change in coordination environment, electronic state, or atomic position—can be directly attributed and mechanistically interpreted. This level of resolution is rarely attainable in conventional nanoparticle catalysis, where broad size and shape distributions obscure atomic-scale details[8,14,31].

In summary, operando spectroscopic characterization has transformed atomically precise nanoclusters from static structural models into dynamic catalytic platforms. By capturing the evolving structure of clusters under real reaction conditions, these techniques provide a direct link between microscopic dynamics and macroscopic function. The ability to visualize how ligands detach, how dopants migrate, and how support interactions reshape the cluster represents a decisive step toward establishing predictive design principles in nanocatalysis. This thesis builds upon such methodologies to investigate the catalytic behavior of thiol-protected

gold nanoclusters, correlating atomically precise structures with their reactivity, stability, and evolution under relevant reaction environments.

1.2 Gas-Phase Reactions in Nanocluster Catalysis: CO Oxidation and the Water–Gas Shift (WGS)

Gas-phase reactions such as carbon monoxide (CO) oxidation and the water–gas shift (WGS) are not only of great technological importance but also serve as benchmark reactions for understanding the structure–activity relationships of nanocluster catalysts. Both reactions are highly sensitive to the surface composition, metal–support interactions, and dynamic restructuring of active sites, making them ideal systems to study with atomically precise nanoclusters.

It is generally accepted that in both CO oxidation and the WGS reaction, CO adsorbs preferentially on metallic sites, while H_2O molecules are activated at oxygen vacancies in reducible oxide supports such as cerium dioxide (CeO_2). The reactions therefore proceed most efficiently at the metal–support interface, where geometric features (oxygen vacancy formation, lattice strain, atom migration) and electronic processes (charge transfer between metal and support) cooperatively modulate reactivity.

CeO_2 is a particularly well-studied support, noted for its ability to stabilize small metal clusters, resist sintering, and mediate oxygen storage and transfer. When combined with noble metals such as Au or Pt, CeO_2 enhances CO adsorption, water activation, and low-temperature catalytic activity. Pt–Au–CeO_2 systems, in particular, have demonstrated outstanding performance under mild conditions, with activity and selectivity highly tunable by cluster size, dopant type, and ligand environment[8,26,32].

1.2.1 CO Oxidation Reaction

CO oxidation:

Equation 1: reaction of CO and O2 to CO2 as the CO Oxidation reaction

$$2\,CO + O_2 \rightleftharpoons 2\,CO_2$$

This is one of the most extensively studied reactions in heterogeneous catalysis and is frequently employed as a model probe reaction. Because of its simple chemistry, it serves as a sensitive diagnostic for catalyst performance and as a platform to explore fundamental questions of adsorption, charge transfer, and interfacial synergy[33]. Beyond its basic environmental relevance in removing toxic CO, it provides mechanistic insights applicable to more complex transformations.

The mechanism of CO oxidation on PtAu nanocatalysts is known to involve multiple competing pathways, with both Langmuir–Hinshelwood (associative adsorption of CO and O_2 prior to reaction) and Eley–Rideal (gas-phase O_2 reacting with adsorbed CO) mechanisms reported, depending on catalyst composition and reaction conditions. Activation energies for CO oxidation on AuPt systems vary widely, from ~55 to 102 kJ/mol, illustrating the sensitive dependence on alloy ratio, support, and structure[33,34].

At the Pt–Au/CeO_2 interface, CO preferentially adsorbs on Pt sites, while lattice oxygen and oxygen vacancies on the ceria supply the oxidizing equivalents. This generates CO_2 while creating oxygen vacancies, which are subsequently replenished by gas-phase O_2, restoring the interface. Alloying Au with Pt enhances this process in several ways[33,35]:

- Au weakens strong CO adsorption on Pt, mitigating poisoning and maintaining turnover.
- Au stabilizes dispersed Pt sites or even single atoms against sintering.
- The Pt–Au interfacial ensemble facilitates charge transfer to CeO_2, enhancing reducibility and accelerating oxygen vacancy formation.

Thus, CO oxidation is not only a model reaction for low-temperature oxidation activity, but also a crucial probe of interfacial oxygen dynamics, directly connecting to the mechanisms central to the WGS reaction.

1.2.2 Water–Gas Shift (WGS) Reaction

The water–gas shift reaction:

Equation 2: water-gas shift reaction, from CO and H2O to H2 and CO2

$$CO + H_2O \rightleftharpoons CO_2 + H_2$$

is a cornerstone in hydrogen generation and purification technologies. It serves dual roles: (i) reducing CO content in synthesis gas streams and (ii) producing high-purity H_2 – critical for sustainable energy applications such as fuel cells. The exothermic nature of the WGS means that, although it is thermodynamically favored at lower temperatures, its kinetics are enhanced at higher temperatures, necessitating catalysts that can bridge this mismatch by lowering activation barriers at mild conditions[22,36].

Au- and Pt-based catalysts supported on ceria have repeatedly demonstrated high performance for WGS[8]. Mechanistically, it is widely accepted that:

- CO adsorbs on metallic Au or Pt sites, often at interfacial positions.
- H_2O dissociates at ceria oxygen vacancies, yielding hydroxyl species and Ce^{3+} centers.

The reactive interface then mediates CO oxidation with either lattice oxygen (redox pathway) or surface hydroxyls (carboxyl pathway)[29].

Despite decades of research, ambiguity remains about the identity of the true active species (metallic vs. cationic Au/Pt, isolated atoms vs. small clusters), and whether the WGS proceeds predominantly via a redox mechanism or a carboxyl intermediate. Recent in situ and operando studies have started to resolve these debates:

X-ray absorption and vibrational spectroscopy confirm that metallic Au^0 and Pt^0 sites remain largely intact, even in oxidative environments, but transient $Au^{\delta+}$ or $Pt^{\delta+}$ interfacial states emerge during turnover[37]. The formation of $Pt^{\delta+}$ –OV–Ce^{3+} interfacial ensembles has been directly linked to enhanced CO chemisorption and H_2O dissociation[37]. DFT calculations show that high-temperature conditions favor the redox pathway (CO oxidation via lattice oxygen after H_2O dissociation), whereas low temperatures promote the carboxyl pathway (formation and decomposition of COOH intermediates)[30]. These insights suggest that the WGS is driven not by isolated metal or support properties alone, but by a synergistic, dynamic interface where metal dispersion, support reducibility, and charge transfer collectively determine the catalytic turnover.

Despite differences in complexity, CO oxidation and WGS are mechanistically connected. Both reactions rely on CO activation on metal sites and O/H activation on ceria oxygen vacancies, and both highlight the role of metal–support interfaces as the true catalytic centers. CO oxidation thus serves as a probe for oxygen activation and vacancy regeneration, providing a diagnostic for the reactivity that underpins WGS.

2 Motivation and Objectives

Although CO oxidation and the water–gas shift (WGS) are among the most studied reactions in catalysis, a true atomic-scale understanding of their mechanisms remains elusive. This is mainly due to the complexity of real catalyst systems, where multiple parameters—ligands, dopants, and support interactions—act simultaneously and obscure precise cause-and-effect relationships.

Atomically precise gold nanoclusters (Au NCs) offer a way to overcome this challenge. Their well-defined structures, tunable ligand shells, and controllable doping make them an ideal platform for disentangling the individual roles of structure, ligation, support interactions, and dopant atoms. By employing these systems in CO oxidation and WGS catalysis, it becomes possible to establish clear correlations between atomic structure, dynamic transformations, and catalytic function.

The aim of this thesis is therefore to develop a deeper understanding of ligand-protected Au nanoclusters in heterogeneous catalysis, using CO oxidation as a probe reaction and focusing on the WGS reaction as a target process relevant to sustainable hydrogen production. In order to achieve this, the thesis is undertaking a comprehensive evaluation on protective ligands regulating the surface accessibility, stability and catalytic activity of nanoclusters. Furthermore, the investigation examines the impact of CeO_2 as a reducible oxide support on cluster stabilization, charge transfer processes and oxygen vacancy dynamics. The present study further explores the impact of heteroatom doping, particularly with Platinum, on the structure and electronic properties of gold clusters, with an insight to tailoring their catalytic capacities and structural dynamics. The monitoring of ligand removal, dopant migration and active site formation under activation and reaction conditions is carried out through the utilization of in-situ and operando spectroscopy. Ultimately, the research aims to correlate precise structural dynamics with catalytic pathways in CO Oxidation and water-gas shift reaction to identify the most effective active site phases. By addressing these objectives, this work seeks to advance the rational design principles of nanocluster catalysts for environmentally friendly hydrogen production.

3 Experimental

3.1 Nanoclusters synthesis

As reported by Negishi [38] et al. Pt Au alloy nanoclusters demonstrated high hydrogen evolution reaction in electrocatalytic cells. To further investigate their performance in catalytic reactions the laboratory of Negishi has provided three differently ligand protected clusters. $[PtAu_{24}(2\text{-phenylehanethiolate})_{18}]^0$ (PET) was synthesized followed Scheme S1[39] from an already reported method and was subsequently used as a precursor to obtain $[PtAu_{24}(4\text{-tert-butylbenzenethiolate})_{18}]^0$ (TBBT) via ligand exchange reaction [38] (Scheme S2[39]). The purity and composition of the isolated product has been confirmed via UV-Vis spectroscopy and electronspray ionization-mass spectrometry (ESI-MS). Serendipitously $[PtAu_{24}(4\text{-tert-butylbenzenethiolate})_{12}(thiodithiolate)_3]^0$ (TDT) was discovered during this high temperature ligand exchange reaction (Scheme S3[39]) leading to a purification of the initial batch and extraction via reverse-phase high-performance liquid chromatography (RP-HPLC) containing only one peak additional to TBBT, confirming a newly found nanocluster and its purity. Single-crystal X-ray diffraction has finally helped to reveal the chemical composition of the newly found cluster, due to the difficulties determining it purely from ESI-MS when originally coming from PET and TBBT cluster. [38]

While all clusters share a common $Au_{12}Pt$ core, in which the central Pt atom is encapsulated by Au atoms and stabilized by (-S-Au-S-Au-S-) staple motifs, their ligand shells differ substantially(Figure 3). This variation in ligand architecture is expected to influence not only the electronic and geometric environment of the active sites but also the interaction of the clusters with the CeO_2 support and reactants.

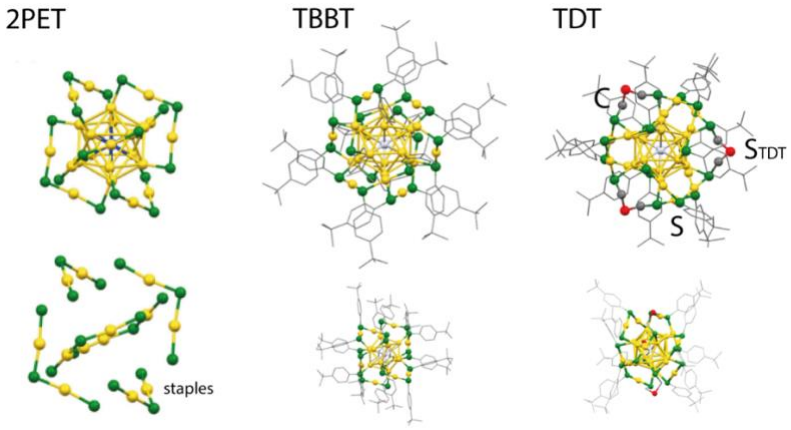

Figure 3: Scheme of the three PtAu24(SR)18 nanoclusters protected by different ligands structure

3.2 Catalyst preparation

The synthesis of ceria consisted of combining 5.63 g of Cer(III)nitrate hexahydrate with 0.1 Pluronic F-127 in 4 mL of ethanol, the solution was steered for 12 h. After adding the solution to a crucible, heating to 350 °C with a 10 °C/min ramp and a hold for 4 h in air have been conducted. The fine formed powder was dried for 24 h, under air at 80 °C before an impregnation was performed. The production for a 0.5 wt% loaded catalyst the correspondent amount of cluster has been dissolved in toluene and mixed with the CeO2. After 12 h of steering in a rotating flask, the solvent was evaporated. The final drying step has been performed at 80 °C under air for 12h.

3.3 Pretreatment methods

Regarding CO Oxidation and Water gas shift reaction the thermal treatment has always been performed right before the reaction to keep the system under inert conditions between the two steps. The same amount of 60 mg of catalyst was used for both reactions and the total flow of 40 ml/min has been kept steady over the study. For CO Oxidation studies a combination of reducing and oxidative atmospherically thermically treatment has been conducted right before reaction. Heating from room temperature to 250 °C was performed with a 10 °C/min ramp in a 5 % O_2 atmosphere in Argon. Under these conditions the catalyst has been kept for 30 min, after a system clean for 10 min at the held temperature with pure Argon flow, a switch to 5 % H_2 in Ar with a hold for 30 min was performed until cooling in Ar to room temperatures. Two types of pretreatment for the water-gas shift were compared, the atmospheric conditions did not differ to the CO Ox. beginning with a 5 % oxygen atmosphere when heating up und holding for 30 min at final temperature. After a system flush with argon for 10 min, 30 min in 5 % hydrogen has been

held until inert cooling to room temperatures. Firstly, pretreatment with a hold at 250 °C was studied, before switching to 300 °C for comparison.

3.4 Catalytic studies

Gas phase CO Oxidation reactions have been performed in a flow reactor with an INFICON micro-GC for analysis, same as the water-gas shift reactions. The gas flows were regulated with Bronkhorst mass flow controllers and the temperature conditions in a cylindrical oven were adjusted by a PID controller with a Ni/NiCr thermocouple placed inside the catalysts bed. The catalyst powder has been placed in a quartz glass tube and held in position with quartz wool plugs. The total flow was always kept at 40 mL/min, the pretreatment has been conducted as stated in the paragraph before. After the thermal treatment the system was stabilized at room temperatures in argon, then the system was introduced to the reaction gas mixture of $CO:O_2$ with a 1:1 ratio, each at 5 % in the total 40 mL/min flow. Reaction temperature was held at 250 °C for 60 min after heating with 5 °C/min (Figure 4). For recyclability runs, the system has been cooled under the $CO:O_2$ mixture to room temperature, cleaned with Ar for 45 min and then started again with a system equilibration to the gas mixture in room temperature until the start of the same temperature profile as before.

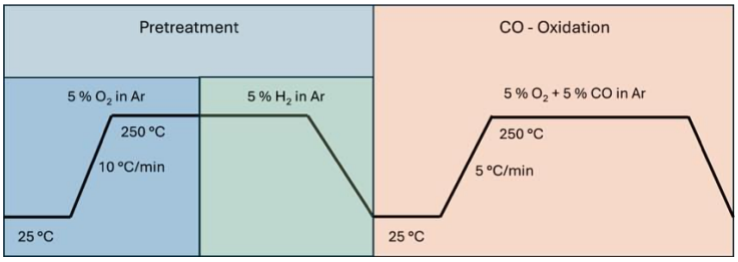

Figure 4: CO Oxidation reaction with pretreatment in O2 and H2 for 30 min each at 250 °C and the reaction with CO and O2 in Argon, both with 10°C/min heating ramp

WGS runs were pretreated as stated in the paragraph before, the instrumental setup has not been modified apart from an additional saturator filled with water in the argon stream which was only used for reaction. After thermal conditioning the system has been equilibrated in the reaction mixture with Ar bubbling through the water filled saturator and a 5 % CO flow. Temperature steps of 250, 300 and 350 °C were used with a 40 min equilibration phase for each, heating of 5 °C/min was used for every ramp (Figure 5). Regarding the recyclability studies, the system has undergone pretreatment and the first reaction on one day, after cooling the catalyst a steady argon flow has

been established to preserve the integrity of the system over night at room temperature until the reaction has been restarted for a second time on the same catalyst.

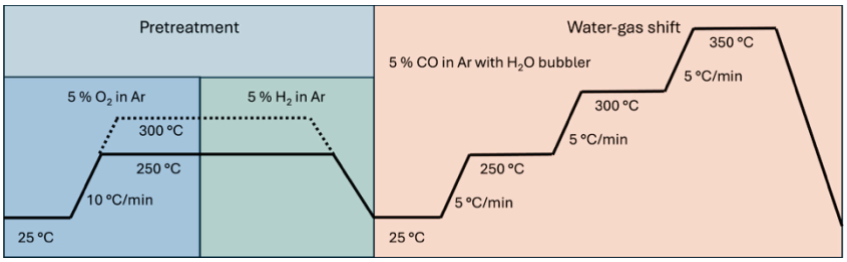

Figure 5: WGS reaction conditions with pretreatment of 250 °C (solid) and 300° (dotted) with same gas configuration, reaction conditions were the same with a hold of 45 min at each temperature step (250, 300 and 350 °C) with 5 % CO and H2O in a bubbler

3.5 Ex situ/In situ spectroscopic studies

3.5.1 Diffuse reflectance infrared Fourier transform spectroscopy (DRIFTS)

DRIFTS studies were performed on a Bruker Vertex 70 spectrometer with a liquid-N_2-cooled MCT detector with a 4 cm^{-1} resolution. A stainless-steel flow cell from Pike technologies has a CaF_2 window and an oven. The cells gas flow was controlled by a MKS Multi-gas controller 647C and the temperature was controlled with X and a Liquid Recirculatory (PIKE Technologies) The samples have been placed into ceramic crucibles with a normalized weight of 10 mg and transferred into the flow cell (PIKE Technologies DIffusIR). The IR spectra were recorded during all the measurements in a 3-minute interval. The background has been taken separately before every CO dosing or reaction step individually. The pretreatment of the samples was performed as described above after a system flush with a 12 ml/min Ar flow. The major difference to the catalytic activity studies, was the reduction of the total gas flow to 13 ml/min due to systems limitations. After the pretreatment the system has been cooled to room temperature under Argon flow. For a surface composition study a 10 % CO flow in argon was established for 30 min, followed by purging with Ar for 30 min to remove the CO in gasphase until no further changes in the IR spectra were monitored. The catalysts were then measured while undergoing WGS reactions with a limiting CO gas-mixture of 5,55 % (due to a limited gas flow controller) and 1,84 % water in Ar, with the same heating scheme as in the kinetic studies. After the reaction, the

system was flushed with Ar and cooled to room temperature, to repeat the CO adsorption experiment.

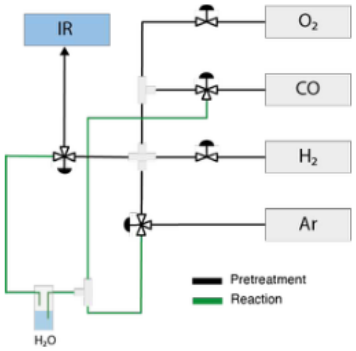

Figure 6: IR DRIFT and CO Adsorption study setup with gas supply: Oxygen, CO, Hydrogen, Argon and a valve configuration for pretreatment / CO Ads experiments as well as WGS reaction DRIFTS[8]

3.5.2 X-ray Absorption Fine Structure (XAFS)

The fundamental principle underling X-ray Absorption Fine Structure (XAFS) spectroscopy is the photoelectric absorption of X-rays by core electrons, influenced by their local coordinating atomic environment. The interference between the outgoing electron and the backscattered wave modulates the absorption coefficient μ(E), providing an element-specific oscillatory fine structure as a function of energy[40]. Conventionally, XAFS are separated in two complementary categories, X-ray Absorption Near Edge Structure (XANES) and Extended X-ray Absorption Fine Structure (EXAFS). For gaining insight into the oxidation states, the coordination geometry and the electronic structure, spectra from the elements absorption edge to 50 eV above it are taken. Further extending from 50 eV to approximately 1000 eV above the edge is attributed to the region of EXAFS, which is considered to provide quantitative local structural knowledge. This includes interatomic distances as wells as coordination numbers and thermal disorder[41].

In conditions that are conducive to the process, EXAFS are capable of providing remarkable precision on the average interatomic distances, coordination numbers and the Debye-Waller factor. Which quantifies thermal as well as static disorder around individual atoms[42]. The frequency of EXAFS oscillations is directly proportional to the photoelectron scattering path length. It is evident that the number and type of backscattering atoms are responsible for the

amplitude of such a signal, with k-dependent backscattering amplitude functions[40] playing a pivotal role in this regard.

The structural analysis of individual systems can be conducted in a variety of environments and scenarios. Ex-situ measurements are defined as those taken from a baseline structural information in a stable state under ambient conditions. In-Situ studies provide insights into simulated reaction condition dependent structures without demonstrating catalytical activity. The detection of dynamic or metastable phases is only achieved under reaction conditions while converting products, and are therefore considered operando XAFS experiments. It is evident that these have provided a paradigm shift in the structural analysis of heterogeneous catalysis and material science[28,43,44].

In situ XAFS measurements were performed at ALBA Synchrotron in NOTOS Beamline in fluorescence mode (Au-L_3 edge and Pt K-edge) in the solid/gas reactor multipurpose cell. The synchrotron light generated by a bending magnet was first vertically collimated, then monochromatized with two pairs of liquid-cooled Si(111) crystals, and finally focused onto the sample area to approximately 500 × 500 μm^2. A combination of silicon and rhodium stripe coatings on the two optical mirrors ensures the rejection of higher harmonics. The catalyst, fresh, pretreated, used and used twice, have been pressed into pellets. For spectra of the pure cluster, drop casting of the clusters in toluene on Kapton tape has been performed for the static ex-suit measurements. XAS data from the electrodes were collected in fluorescence mode using a 13-element Si drift detector from Canberra.

Data reduction has been done according to standard procedure by using the Demeter XAS program suite[45]. Extended X-ray Absorption Fine Structure (EXAFS) spectra have been analyzed in the k square and in the range 3 to 12 $Å^{-1}$. Theoretical model paths for further data analysis were generated using the FEFF6 code[46]. A two-shell model, incorporating contributions from Au-S and Au-Au, was employed for data refinement, adjusting coordination numbers, distances, and disorder factors. To achieve a more robust determination of these parameters, we conducted a unique fit on the 9 spectra (8 samples spectra plus the Au foil one). For each spectrum in the dataset, we considered two coordination numbers (N Au-S and N Au-M, where M = Au or Pt) and two correction factors for interatomic distances (δR Au-S and δR Au-M) as fitting parameters. Given the limited k range and the strong inter-correlation among the fitting parameters, we opted to use only two disorder parameters (σ^2Au-S and σ^2Au-M, plus σ^2Au-Au for the foil), which were

kept common across all spectra in the dataset. The passive electron reduction factors S_0^2 has been taken directly from Au foil. This strategy ensures that the coordination numbers derived from the analysis are consistent with all available experimental data. Finally, we fitted the energy correction to the photoelectron reference ΔE_0, which is also common to all spectra.

4 Results and discussion

The three atomically precise bimetallic nanoclusters investigated in this study — $Au_{24}Pt$(2-phenylethanethiolate)$_{18}$ (PET), $Au_{24}Pt$(4-tert-butylbenzenethiolate)$_{18}$ (TBBT), and $Au_{24}Pt$(4-tert-butylbenzenethiolate)$_{12}$(thiodithiolate)$_3$ (TDT) — were synthesized and characterized based on previous experience[38]. While all clusters share a common $Au_{12}Pt$ core, in which the central Pt atom is encapsulated by Au atoms and stabilized by (-S-Au-S-Au-S-) staple motifs, their ligand shells differ substantially. This variation in ligand architecture is expected to influence not only the electronic and geometric environment of the active sites but also the interaction of the clusters with the CeO_2 support and reactants. Previous reports have suggested that the Pt atom, initially located at the center of the cluster, may migrate towards the surface under reaction conditions, potentially altering catalytic performance[8]. To systematically investigate the impact of ligand environment on catalytic behavior, all three clusters were supported on CeO_2 via wet impregnation, maintaining a consistent metal loading of 0.5 wt%.

4.1 Catalytic activity in CO and WGS reactions

The influence of ligand configuration on CO oxidation reactivity was evaluated following a combined oxidative and reductive pretreatment at 250 °C. To assess catalyst durability, recyclability tests were performed by cooling the reactor under Ar, then repeating the reaction cycle without replacing the catalyst. Reproducibility was confirmed using freshly prepared catalyst batches subjected to identical pretreatment and reaction protocols.

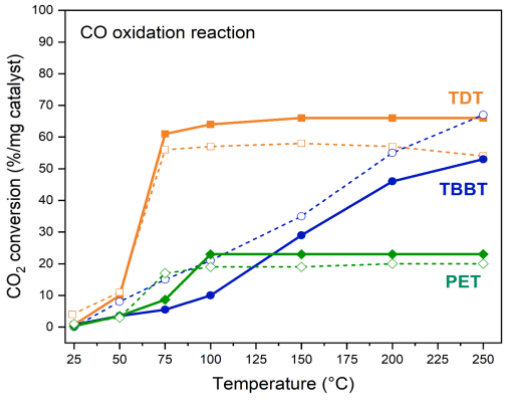

Figure 7: CO Ox. Catalytic activity of PtAu24 nanocluster catalysts supported on CeO2 (solid = first run ; dotted = second run)

The results, summarized in Figure 7, demonstrate clear differences in catalytic performance depending on the ligand environment. Among the three systems, the TDT-protected cluster exhibited the lowest activation temperature, achieving notable CO conversion as early as 50 °C and reaching a maximum of 66% at 75 °C, indicating superior low-temperature activity. The TBBT-protected cluster also initiated conversion at low temperatures but exhibited a more gradual increase in activity with rising temperature, achieving a moderate final conversion. In contrast, the PET-protected cluster showed a delayed onset of catalytic activity, with maximum CO conversion of only 23% at 100 °C, suggesting poorer accessibility of active sites or less favorable metal-support interactions. Catalyst stability was further investigated through repeated reaction cycles. The PET-protected catalyst exhibited the highest stability, with minimal activity loss upon reuse. The TDT-based catalyst showed approximately 10% decline in activity, indicating moderate deactivation. Low activation energy has maintained over the second cycle with only the maximum conversion plateauing at 55 %. Interestingly, the TBBT-protected cluster displayed an increase in activity during the second cycle with already surpassing conversion at low temperatures, suggesting a possible activation or restructuring effect under reaction conditions. This may improve the accessibility of active sites or enhance interfacial contact with the CeO_2 support.

Building on the insights gained from CO oxidation, we next evaluated the performance of the same ligand-protected $Au_{24}Pt$ nanocluster catalysts in the WGS reaction. This allowed us to directly compare how ligand type and thermal treatment influence catalytic activity across two mechanistically related but distinct reactions. As with CO oxidation, the catalysts underwent oxidative and reductive pretreatments, this time at maximum temperatures of either 250 °C or 300 °C. The WGS reaction was conducted by ramping the temperature at 5 °C/min to 250 °C (holding for 40 min), then sequentially to 300 °C with similar dwell times. Recyclability was assessed by cooling the catalyst to room temperature after each run and repeating the reaction cycle. Since the reaction runs included the heating to 300 and 350 °C already in run one, though the catalysts not having been exposed these thermal environments not data has been displayed due to the hypothesis of restructuring during this time, which would provide non representative results.

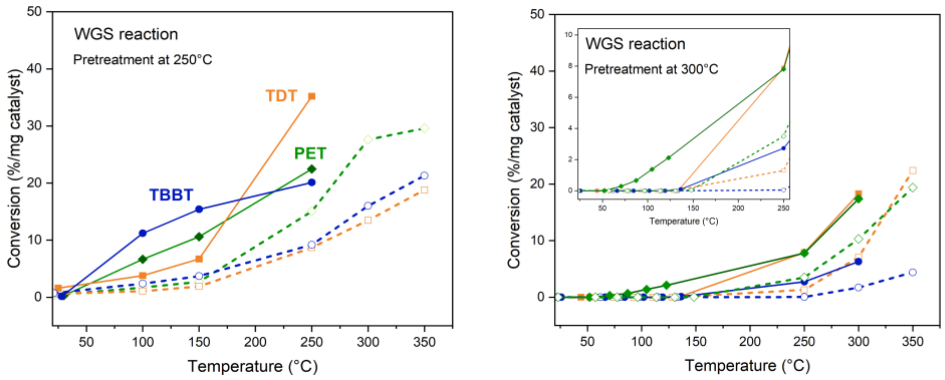

Figure 8: WGS Catalytic activity of PtAu24 nanocluster catalysts supported on CeO, (solid = first run ; dotted = second run)

The results (Figure 8) reveal that all three catalysts exhibit good WGS activity following a 250 °C pretreatment, with the TDT cluster again outperforming its counterparts—mirroring the trend observed in CO oxidation. Notably, TDT was the only catalyst to achieve a conversion of 35% under these conditions. Focusing on the activation temperatures a direct inversion of low temperature conversion is observable, TDT being the last sample to surpass the 5% conversion barrier. Interestingly, the PET-protected cluster, which showed the slowest activation and lowest conversion in CO oxidation, did not display the expected stalling in WGS; instead, it outperformed the TBBT sample, achieving a maximum conversion of 29.6% at 350 °C in the second cycle. Surpassing the prior catalytic performance was not observed in any of the samples at same temperatures. PET increasing its performance when detecting the gas flow at higher temperatures, whereas TBBT only equaled the same numbers from before. However, increasing the pretreatment temperature to 300 °C led to a marked decrease in both conversion rates and overall activity for all clusters, suggesting that higher thermal exposure in oxidative and reductive environments may induce irreversible structural changes detrimental to catalytic performance. This effect was particularly pronounced for the TDT and TBBT samples. In the first cycle of TDT after 300 °C pretreatment the maximum conversion was not only cut by nearly 13 % at the thermal conditioning temperature, furthermore the conversion at only 250 °C decreased to single digit numbers. TBBT also demonstrated a similar reduction in catalytic performance, only PET revealed the highest stability over tougher thermal conditioning, resulting in minor performance reduction.

Recyclability studies further highlighted the dynamic nature of these catalysts. After the first reaction cycle, both PET and TDT clusters showed improved conversion at 350 °C compared to their initial runs, with PET reaching 19.4% (up from 17.4%) and TDT achieving 22.4% (compared

to 18.8% after a 250 °C pretreatment). In addition, TDT as well as PET outperformed their first cycles after 300 °C conditioning. TBBT shows to take the highest influence of thermal conditioning, deteriorating the H_2 production further the harsher the environment. These observations suggest that initial thermal cycling may facilitate structural rearrangements that enhance active site accessibility or stability, particularly for the TDT cluster. PET seems to be the least affected by its recycling as well as a variety of thermal conditioning, correlating the high stability from CO Oxidations with the relentless conversion in WGS.

All of these findings highlight the intricate relationship between ligand environment, heat treatment, and catalytic performance in atomically precise PtAu nanoclusters. The enhanced activity and versatility of the TDT-protected cluster in CO oxidation and WGS reactions suggests that the structure of the ligand plays a crucial role in determining the activity and stability of PtAu nanocluster catalysts on CeO_2, potentially by influencing metal-support interactions, active site exposure and surface dynamics. A deeper understanding of the structural dynamics under reaction conditions is essential to fully unravel these influences.

4.2 Structural evolution by pretreatment and CO oxidation

To elucidate the structural evolution of active sites on the Pt-Au-Ceria system CO Adsorption studies been conducted after oxidative/reductive pretreatment (indicated by the dotted lines in Figure 9) and after reaction (solid line)

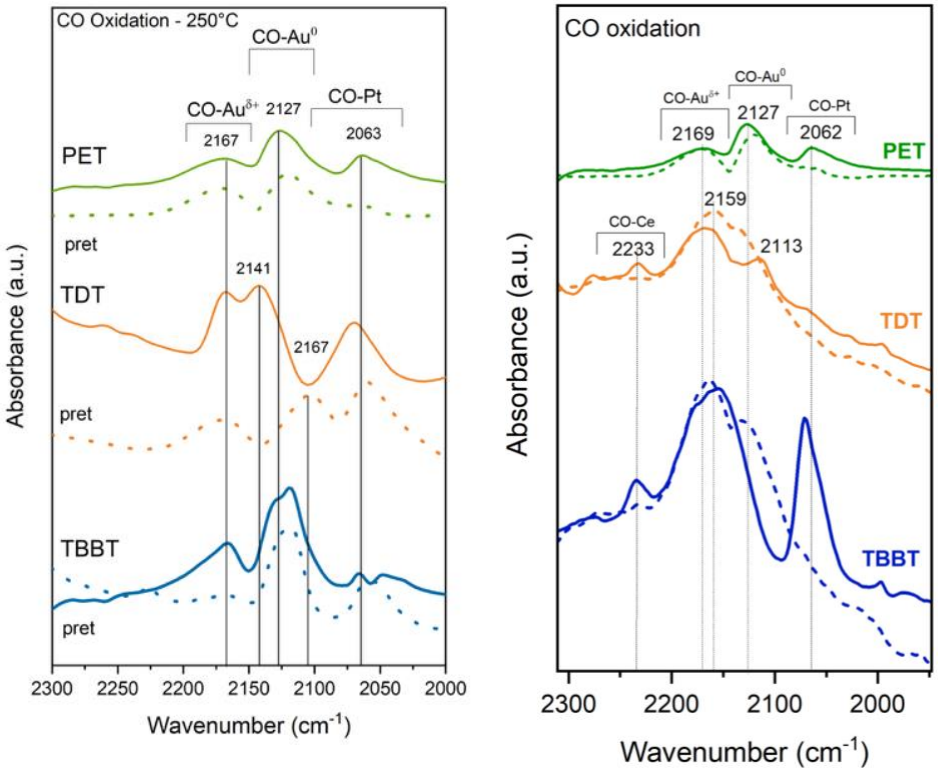

Figure 9: CO-IR spectra after pretreatment (dotted) and after reaction CO oxidation (solid) with pretreatment at 250 °C on the left and 300 °C on the right

The DRIFTS spectra reveal distinct vibrational signatures corresponding to CO adsorbed on both Au and Pt sites, with band positions and intensities reflecting the oxidation states and local environments of these metals. Notably, the data indicate significant restructuring of the clusters during from the pretreatment to after reaction conditions depending on the ligand.[8,16,17,25,26] For the PET cluster, two prominent Au–CO bands were observed at 2127 cm^{-1} and 2169 cm^{-1}, with the 2127 cm^{-1} band being more intense. The band at 2127 cm^{-1} is associated with CO adsorption on neutral Au atoms, while the higher-frequency band at 2169 cm^{-1} is attributed to CO bound to partially oxidized Au ($Au^{\delta+}$). Additionally, a band at 2062 cm^{-1} is assigned to CO linearly adsorbed on Pt sites[35], supporting the migration and surface exposure of Pt during pretreatment and more pronounced after reaction. Importantly, the PET cluster displayed the least spectral change upon reaction, with only an increase in band intensity related to the CO on Pt sites.

In contrast, the TDT sample exhibited more pronounced structural changes throughout the catalytic process. After pretreatment, the DRIFTS spectra displayed overlapping bands between 2160 and 2120 cm^{-1}, indicative of multiple Au oxidation states and suggesting a higher proportion of cationic Au species relative to metallic Au. A low-intensity band around 2060 cm^{-1}, corresponding to CO adsorption on Pt sites, was also observed and increased in intensity

following CO oxidation, similar to the trend seen for the PET sample. After the catalytic reaction, a pronounced band at 2113 cm^{-1} emerged, which can be assigned to CO adsorbed on metallic Au, while the intensity of the bands associated with cationic Au decreased. Notably, a new band appeared at 2233 cm^{-1}, which is attributed to CO adsorption on Ce^{4+} sites — a feature not observed in the other samples. This high-frequency band may reflect a unique interaction between the TDT ligand and the ceria support, potentially altering the surface properties and accessibility of Ce^{4+} sites[47]. A similar trend was observed for the TBBT-protected cluster. After pretreatment, the DRIFTS spectra revealed a predominance of cationic Au species, as indicated by strong bands in the higher wavenumber region, along with overlapping features attributable to metallic Au. Following the catalytic reaction, a broad and intense band emerged between 2020 and 2110 cm^{-1}, which can be assigned to CO adsorbed on both Pt sites and metallic Au. This band is distinct from the higher wavenumber features associated with more cationic Au species, suggesting a redistribution of surface species and an increase in the proportion of reduced, metallic sites after reaction[37].

To gain deeper insight into the structural stability and ligand dynamics of $PtAu_{24}$ nanoclusters protected with different ligand types, we performed static X-ray absorption fine structure (XAFS) spectroscopy at the Au L_3-edge under various experimental conditions: as-synthesized, after thermal pretreatment, and following CO oxidation catalysis. The two ligand systems, single-ligand protection with tert-butylbenzenethiolate (TBBT) and a mixed-ligand system containing both TBBT and thiodithiolate (TDT) were investigated. Given the distinct protection motifs compositions imparted by these ligands, differences in the structural response during activation and reaction were already detected by the CO infrared experiments and further confirmed by the R-space fitting results (Figure 10).

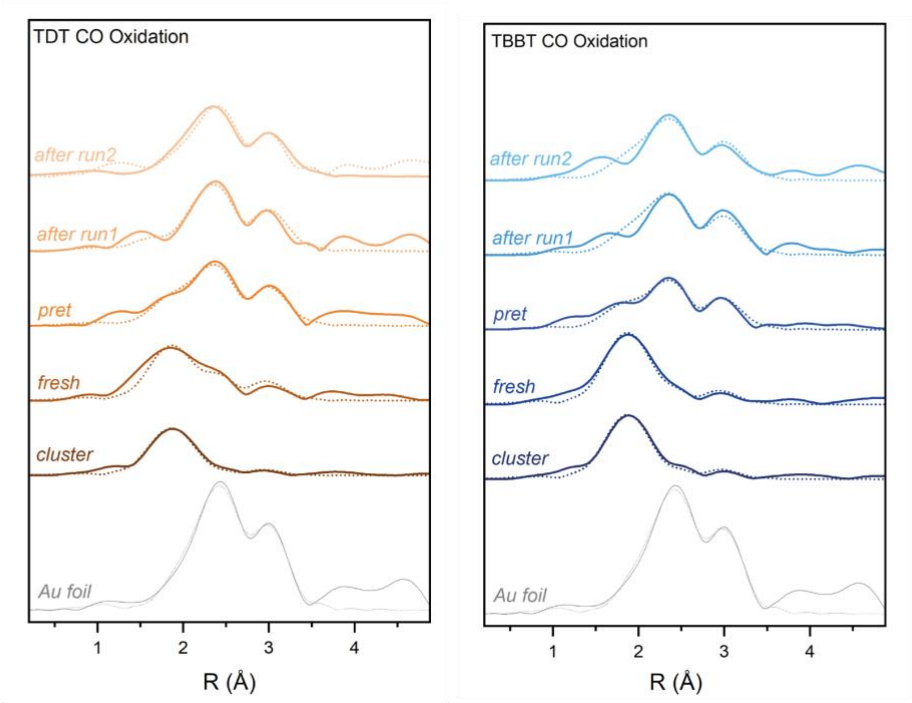

Figure 10: EXAFS R space at Au L3-edge including fitting (dotted lines and table).

Table 1: EXAFS R space at Au L3-edge atomic distances

		Au-S		Au-Au/Pt	
		N	R	N	R
TBBT	*Cluster*	1.12 ± 0.68	2.31 ± 0.04	1.93 ± 0.68	2.79 ± 0.09
	Fresh	1.27 ± 0.62	2.30 ± 0.09	2.73 ± 0.85	2.77 ± 0.21
	Pret	0.27 ± 0.36	2.27 ± 0.36	6.87 ± 0.81	2.80 ± 0.08
	Run1	0.14 ± 0.78	2.34 ± 0.19	8.54 ± 0.80	2.82 ± 0.10
	Run2	0.14 ± 0.33	2.30 ± 0.50	8.57 ± 1.00	2.82 ± 0.11
TDT	*Cluster*	0.88 ± 0.40	2.30 ± 0.30	1.06 ± 0.65	2.77 ± 0.07
	Fresh	0.91 ± 0.33	2.30 ± 0.18	4.08 ± 0.95	2.79 ± 0.22
	Pret	0.25 ± 0.32	2.30 ± 0.93	8.57 ± 0.98	2.82 ± 0.15
	Run1	0.21 ± 0.92	2.30 ± 0.24	9.20 ± 0.90	2.82 ± 0.15
	Run2	-	-	9.71 ± 0.80	2.83 ± 0.15

For both ligand-protected systems, the XAFS analysis reveals a decrease in intensity and bond distance of the Au–S coordination peak upon thermal activation[7,8,16,17]. This is indicative of a partial loss of thiolate ligands from the nanocluster surface. In the case of the TDT-protected clusters, this change is more significant, suggesting a higher degree of ligand detachment or rearrangement. The presence of thiodithiolate, known for a more flexible bidentate coordination mode, may contribute to a less rigid protective shell, making it more susceptible to decomposition or reconfiguration upon heating.

Despite these changes, residual Au–S contributions remain evident even after reaction, particularly in the TBBT-protected sample. The persistence of these signals, albeit weakened and shifted to shorter distances (approaching ~2.2 Å), suggests that some staple motifs are retained on the cluster surface. These findings are consistent with prior reports that partial ligand loss leads to staple unit collapse or reorganization onto the metallic core, rather than complete shell dissociation. Importantly, the continued presence of residual Au–S features support the hypothesis that not all sulfur atoms are removed during thermal treatment or catalysis. [8,26,27]

Following pretreatment, an increase in Au–Au bond contributions was observed in both systems in conjunction with ligand loss. These features remained stable after CO oxidation, indicating the formation of a more metallic gold framework during activation. This structural evolution suggests that, during pretreatment in inert or mildly oxidative environments, vacant coordination sites are generated on the surface as thiolate ligands desorb, thereby enabling new Au–Au interactions to form. The stability of these Au–Au coordination shells throughout multiple catalytic cycles confirms that the metallic core of the cluster remains structurally intact. There was no evidence of cluster agglomeration or growth, as would be indicated by significant increases in coordination numbers or broader distance distributions. The structural fingerprint retained throughout the reaction cycle strongly supports the conclusion that both TBBT- and TDT-protected $PtAu_{24}$ nanoclusters are resistant to sintering or fragmentation under the tested conditions.

While the overall structural integrity of the cluster core is maintained in both systems, differences between ligand types influence the extent of surface dynamics. TDT-containing clusters exhibit a more pronounced reduction in the Au–S signal, likely due to the nature of the mixed ligand configuration possible influence on Au–S bond strength. In contrast, TBBT-protected clusters show more gradual changes, reflecting enhanced stability of different S presence in the motif under oxidative environment.[48,49] These differences have implications beyond structural considerations, impacting the distribution and accessibility of active sites during catalysis. Greater ligand flexibility or fragility, as seen in the TDT system, may offer an accelerated exposure of catalytically active surface atoms, potentially enhancing reactivity. However, this may also lead to a less controlled or heterogeneous surface composition—affecting long-term stability. The TBBT system, while potentially slower in exposing active sites, may offer a more uniform activation process in long-term, as observed in the catalytic activity (Figure 7).

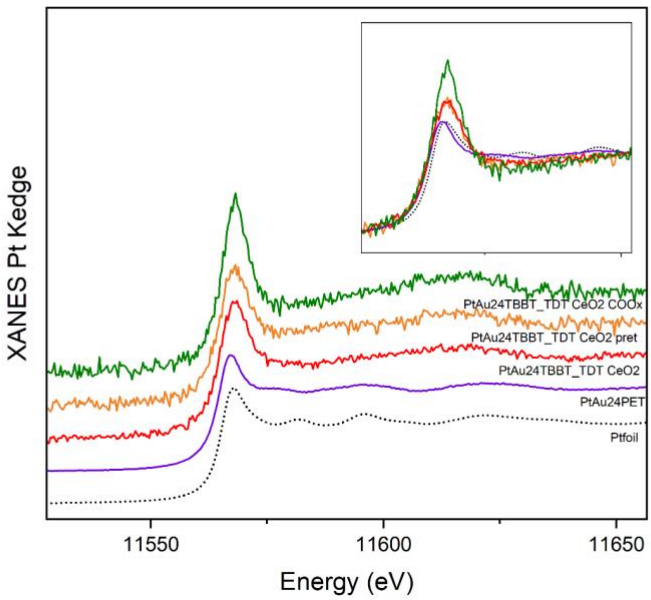

Figure 11: XANES at Pt L_3 -edge including fitting (dotted lines) comparing PET (pure cluster) with TDT (supported = red; pretreated = orange; reacted = green)

In addition, an attempt was made to study the Pt L_3-edge to gain further insights on the Pt dynamics. However, due to the proximity between the energies of Au L_3 and Pt L_3 and the atomic ratio of 1:24 between the two elements (Pt to Au), the measurements were challenging and a proper analysis and separation of the contributions of both metals was not possible. A preliminary analysis of the PET sample (pure cluster) revealed comparatively strong signal in comparison to TDT which were all supported on CeO_2. It can thus be concluded that the low signal intensity is attributable to the loading of only 5 wt.%. As evidenced in Figure 11, the XANES from the samples acquired at the Pt L_3 -edge demonstrates the potential for acquiring knowledge and thereby presents the metallic state of the Pt over the various samples and different histories.

4.3 In-situ DRIFT studies of CO Oxidation reactions

To further understand the activation and conversion from the kinetic studies (Figure 7), in-situ DRIFT studies have been conducted during CO Oxidation reactions after pretreating at 250 °C, as in Figure 4. The catalytic activity can be directly related to the reduction of CO bands (1900 - 2200 cm^{-1}) and CO_2 (2400 - 2300 cm^{-1}). Early activation can be observed with all three samples, close to room temperature.

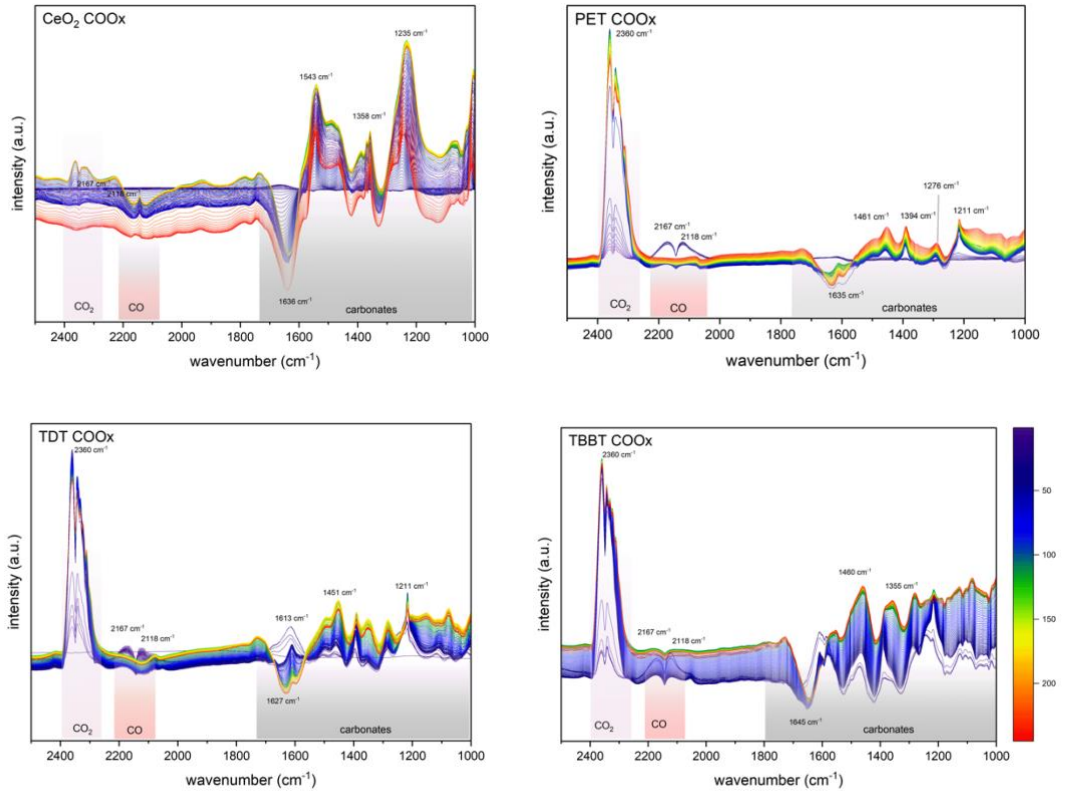

Figure 12: DRIFT COOx ceria blank, PET, TDT and TBBT 2500-1000 wavenumber and temperature scale from 25 °C (blue) to 250 °C (red)

The jump of CO_2 signal detected with the mass spectrometer (Figure 7) of PET can again be visualized with the sudden increase in carbon dioxide band intensity within two scans. The bottoming out after early activation can again be seen. TDT and TBBT activating at low temperatures and therefore confirming kinetic data is also observable.

Apart from the catalytic activity further intermediate formations can be observed in the wavenumber region of 1800 and 1300 cm^{-1} that correspond to carbonates and the symmetric and asymmetric O-C-O stretching vibrations, providing further identification of intermediates formed upon the interaction of CO, O_2 and active sites. Carbonate species with their bands in 1510-1550, 1450-1490 and 1050-1100 cm^{-1} are therefore seen as possible intermediates or spectator species on the catalyst. A blank run of pure ceria, which has undergone the same thermal and gaseous conditions as the loaded samples has shown the same carbonate formation bands as well as the band at 1625-1645 cm^{-1}. With the PET and TDT sample there are distinct band spikes at 1211 cm^{-1}, which are also visible with the TBBT sample, to a lower extend. These bands in the range of 1100–1200 cm^{-1} are assignable to sulfur related species when working with PtAu(SR)/CeO_2 systems. Strong bands in 1050-1160 cm^{-1} are non visible in the blank sample, but distinct for the

nanocluster catalysts and are therefore attributed to the ligands in the thiolated shells. Stretching vibrations of S-O and possible S-C stretches where sulfur coordinates to metal centers and/or oxygen atoms on the support surface are present at lower temperatures and decrease with heating above 100 °C, which therefore confirms the detachment of ligands.

4.4 Surface evolution by WGS reaction

When comparing the three PtAu nanocluster catalysts (PET, TBBT, and TDT) after pretreatment at 250 °C and subsequent water-gas shift reaction (Figure 13), several distinct trends emerge in the CO adsorption profiles. Across all samples, a persistent shoulder near 2085 cm^{-1} is observed after reaction. This feature, which falls within the overlapping region of Pt–CO and Au–CO adsorption, is primarily attributed to linearly adsorbed CO on metallic or cationic Pt sites, including small clusters or single-atom configurations. Previous studies have shown that on Pt/CeO_2, linear CO adsorption on cationic Pt single atoms ($Pt^{\delta+}$) typically appears near 2085–2090 cm^{-1}, while for more reduced or metallic Pt, or for smaller clusters, the band can shift further down to the 2020–2060 cm^{-1} range. [50] For PET and TBBT, only low-intensity Pt-specific bands around 2160 cm^{-1} are detected, which are also associated with linear CO adsorption on more oxidized Pt sites. In contrast, the TDT catalyst displays two strong bands at approximately 2025 and 2170 cm^{-1}. The lower-frequency band at 2025 cm^{-1} can be assigned to CO adsorbed on reduced or metallic Pt sites, while the higher-frequency band at 2170 cm^{-1} may correspond to CO on cationic Pt, but could also indicate CO adsorption on Ce^{4+} sites of the ceria support, as reported in the literature.[50]

For the PET catalyst, the data indicate a predominance of metallic Au on the surface, consistent with trends observed in CO oxidation studies. After reaction, new ceria-related CO adsorption bands also appear, suggesting increased interaction between the cluster and the support, leading to modifications. However, PET continues to show a lower proportion of cationic Au compared to metallic Au, even after higher-temperature pretreatment (300 °C), where a distinct CO–Pt band at 2054 cm^{-1} emerges (Figure 13). The TBBT catalyst, both after pretreatment and after reaction, consistently displays a higher tendency for cationic Au species on the surface. This behavior mirrors its performance in CO oxidation at 250 °C, where cationic gold was also predominant. The stability of these cationic sites is likely influenced by the specific ligand environment provided by TBBT. Interestingly, after reaction at 300 °C, TBBT shows an increase in metallic Au sites, making its surface structure more similar to that observed for CO oxidation after

250 °C pretreatment. For TDT, both CO oxidation and WGS experiments reveal a balanced presence of neutral and cationic Au sites after reaction, suggesting that the TDT ligand environment supports leads to higher stability. Notably, after 300 °C pretreatment, TDT does not show significant shifts in band positions, but rather changes in intensity, reflecting an increase in both CO–Pt and cationic CO–Au bands relative to metallic CO–Au. This indicates that the previously observed balance between charged and neutral Au sites is disrupted at higher pretreatment temperatures, leading to a more dynamic and potentially more catalytically active surface.

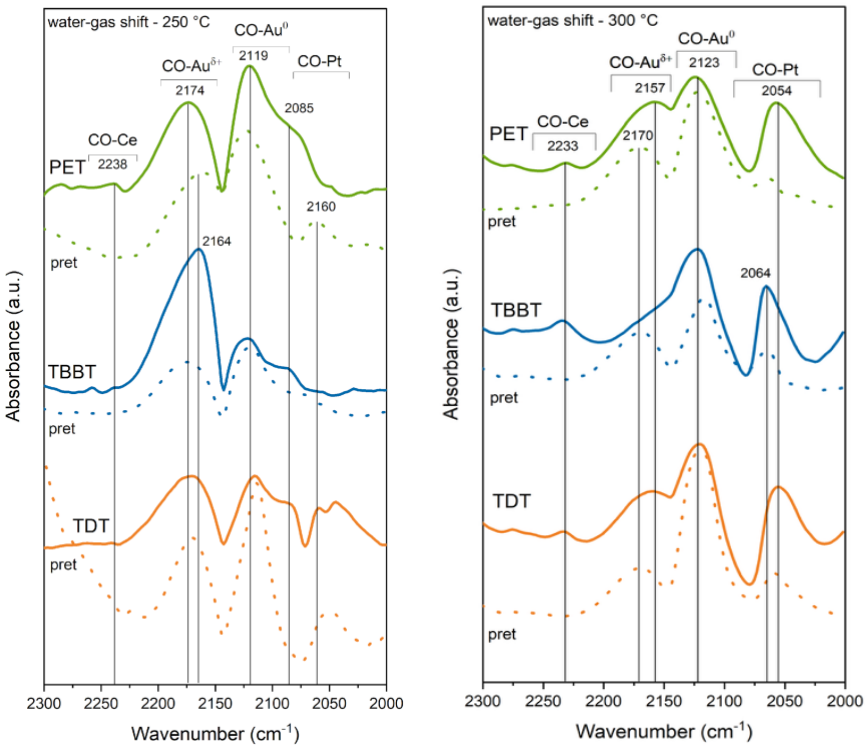

Figure 13: CO-IR spectra after pretreatment (dotted) and after reaction WGS oxidation (solid).

After pretreatment at 300 °C and subsequent WGS reaction, the surface structural changes observed between these two steps are less pronounced compared to those seen with 250 °C pretreatment. Across all three catalysts, the main trends are maintained: there is a marked increase in the CO–Pt band around 2054 cm^{-1} and a greater prevalence of metallic Au, as indicated by the dominance of lower-wavenumber Au–CO bands. Upon exposure to WGS reaction conditions, all catalysts develop a new band at 2233 cm^{-1}, attributed to CO adsorption on Ce^{4+} sites. This feature, also observed after CO oxidation, is even more pronounced following WGS, suggesting enhanced ceria surface activation under these conditions.

4.5 In situ DRIFT studies during WGS reaction

The three different ligand shells leading to different protective motifs configurations lead to different structural evolution observed, mainly related to the evolution of these protective motifs due to their interaction with the support surface, the pretreatment and further under the reaction conditions, whereas the main core structure of the cluster is almost not altered, besides the migration of the Pt atom to the surface core. To further investigate the effect on the catalytic activity, already observed in the kinetics experiments (Figure 8), in situ DRIFTS studies were performed during the WGS reaction, with the catalysts pretreated at 300 °C and shown in **Error! Reference source not found.**. The catalytic activity is strongly related to the evolution of the bands in the region of CO (1900-2200 cm^{-1}), CO2 (2400-2300 cm^{-1}) and OH (3000-3600cm^{-1}). With the three samples the activity is already slowly starting from room temperature with more pronounced increase after 150 °C till 300 °C. Around 250 °C started to be visible the band around 2025 cm^{-1} related to CO, denoting as the CO is reacting in addition on the Au sites also in the Pt sites, in agreement with the catalytic activity results.

The catalytic activity is also denoted in the OH region arising from water dissociation on ceria. Active –OH groups (type-II OH, ~3638 cm^{-1}), which are linked to partially reduced ceria (Ce^{3+}), display changing intensities depending on temperature. The redistribution of these bonds—observed as both negative and positive bands in difference spectra—reflects the ongoing reduction and oxidation of ceria during WGS. These reactive hydroxyls are preferentially formed at the narrow perimeter around metal–ceria interfaces and are implicated in water activation step.

Infrared spectra also reveal characteristic bands associated with formate species adsorbed on the ceria support. Specifically, bands around 2840 cm^{-1}, present in the three samples, are attributed to the C–H stretching vibrations of bidentate formate species, consistent with previous studies on ceria-based catalysts.[51,52] These formates accumulate preferentially on the ceria surface following partial reduction of Ce^{4+} to Ce^{3+}. Supporting the progressive decrease in the OH-related bands indicates cerium reduction upon heating the samples.

Additional prominent bands between 1800 and 1300 cm^{-1} correspond to the symmetric and asymmetric O–C–O stretching modes of surface formate ($HCOO^-$) and carbonate species,

providing a spectral fingerprint of both transient and more stable intermediates formed upon interaction of CO_2 and H_2O with the catalyst surface. During the WGS reaction, these formate and carbonate vibrational bands are directly linked to essential mechanistic steps on catalysts.

Formate species, observed via IR bands near 1580–1600 and 1350–1380 cm^{-1}, serve as key reaction intermediates. According to the widely accepted associative mechanism, CO reacts with surface hydroxyl groups or lattice oxygen from ceria to form bidentate or monodentate formates. These intermediates subsequently decompose, generating H_2 and leaving behind carbonate or carboxylate species bound to the support. Carbonate species, detected by bands near 1510–1550, 1450–1490, and 1060–1100 cm^{-1}, may either represent active intermediates or relatively stable spectator species.[21,51,52] While carbonates tend to dominate at lower temperatures, raising the temperature favors formate species and eventually leads to a more direct redox reaction pathway.

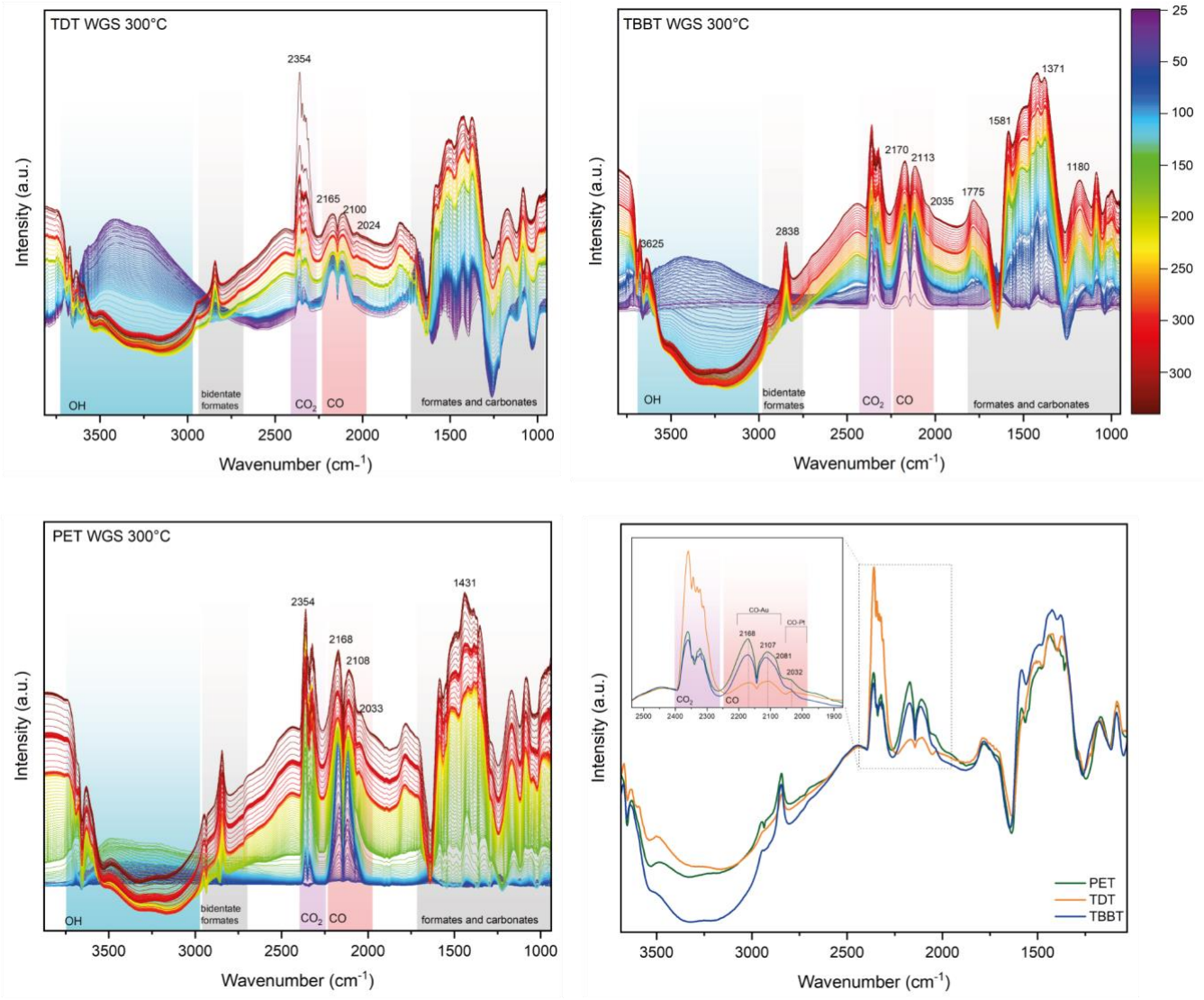

Figure 14: In situ DRIFT experiment with the three PtAu24 nanocluster catalysts pretreated at 300°C and the comparison of the spectra at 300°C under reaction conditions.

In addition to carbonate species, the IR region between approximately 1100 and 1200 cm^{-1} in PtAu(SR)/CeO_2 catalysts can also contain vibrations arising from sulfur-related species. Specifically, strong bands observed between 1050 and 1160 cm^{-1} are primarily attributed to stretching modes involving the sulfur ligands present in the thiolate shell. These include S–O stretching vibrations characteristic of sulfoxide and sulfone functionalities as well as possible S–C stretches where sulfur coordinates to metal centers and/or oxygen atoms on the support surface. [53]

While the formate bands, particularly the symmetric and asymmetric O–C–O stretches, tend to be strong, sharp, and reliable markers for surface reaction intermediates, carbonate bands typically exhibit broader features that may overlap with formate signals. Importantly, the

symmetric stretching and out-of-plane bending modes of carbonate species usually appear at somewhat lower wavenumbers, frequently in the 1100–900 cm^{-1} region.

5 Conclusion

The thesis has investigated the catalytic behavior of three significantly different ligand protected $PtAu_{24}$ nanoclusters supported on CeO_2. The main objective were the catalytic studies and structural evolution over CO Oxidation reaction as well as water-gas shift reaction with thermal conditioning. The results reveal that the activity, stability and structural development of the catalysts are jointly governed by ligand chemistry, thermal preconditioning and support interactions. The mixed ligand protected cluster, TDT, demonstrated the highest level of activity achieving 66 % conversion at 75 °C in CO Oxidation studies. Particularly in the instance of initial thermal cycling, which enhanced active site accessibility. After the first reaction cycle, a 10 % decrease was observed. The best-known ligand type, PET, demonstrated the highest structural robustness and performed consistently over repeated cycles. In the context of TBBT, there was an evident substandard conduct, marked by a gradual activation process that was concomitant with balanced catalytic activity. Similar trends were observed during water-gas shift reactions with TDT again outperforming its counterparts. PET indicated better reactivity than TBBT with achieving 29,6 % conversion while maintaining structural integrity. Increasing thermal exposure prior reaction resulted in decreased catalysis for all systems, notably PET and TBBT showing significant deterioration with an initial thermal cycling.

Spectroscopical analysis revealed that all samples have undergone structural restructuring during pretreatment and catalysis, although to varying extent. TBBT exhibited an increase in cationic Au species over reaction, similar to TDT; whereas PET was excluded from that. Only TDT hinting a unique interaction between ceria and the gold-ligand complex demonstrating Ce^{4+}-sites with CO adsorption studies. In contrast, PET showed the least structural evolution which correlated with the high recyclability observed in the kinetic test. XAFS studies revealed high rearrangement and ligand detachment with TDT, whereas TBBT maintains some staple motifs, resulting in a partial ligand loss. The slower structural evolution of TBBT can be indicative of a more uniform activation process in the long term, as observed in kinetic test. In contrast of the findings in the CO Ox. studies the emergence of Ce^{4+}-CO species were exclusive to TDT, the results of WGS revealed the presence of these species in all three samples. It has been demonstrated that an increase in Pt-CO bands is becoming increasingly decisive for WGS. To be precise, the presence of CO adsorbed on Ce^{4+} sites and the temperature dependent formation of carbonate and formate intermediates provided deeper understanding into the reaction processes. To conclude, incorporating ligand detachment and surface rearrangement, exhibited

a profound influence on catalytic pathways as well as intermediate formation. Combining the findings from the kinetic and spectroscopical studies further emphasize the dynamic nature of nanocluster catalysis and highlight the significant importance of ligand engineering in tailoring performance for CO conversion and hydrogen producing reactions.

Consequently, further research should focus on optimizing pretreatment strategies to inhibit undesired structural evolution while maintaining steady activity over multiple cycles. Ligand design and protection with increased thermal stability as well as controllable detachment properties would allow greater durability in higher thermal environments. The implementation of operando spectroscopy is highly recommended in order to track active site evolution during changes in thermal and gaseous atmospheres. Thereby establishing a direct correlation between structural dynamics and catalytic performance. Finally, it is imperative to expand this research to incorporate further supports, metal atom doping and ligand configurations as well as combinations in order to transition atomically precise nanocluster catalysis from the laboratory to the industrial scale.

6 Bibliography

1. Somorjai, G. A. *Introduction to Surface Chemistry and Catalysis*. (Wiley, New York, NY [u.a.], 1994).
2. Introduction to Catalysis - Chemistry LibreTexts. https://chem.libretexts.org/Bookshelves/Inorganic_Chemistry/Supplemental_Modules_and_Websites_(Inorganic_Chemistry)/Catalysis/Introduction_to_Catalysis.
3. 'EXPLORING THE ROLE OF SURFACE AREA IN HETEROGENEOUS CATALYST ACTIVITY'.
4. Arnaut, L. G. & Formosinho, S. J. Understanding Chemical Reactivity: The Case for Atom, Proton and Methyl Transfers. *Chem. Eur. J* **14**, 6578–6587 (2008).
5. Roduner, E. Understanding catalysis. *Chem Soc Rev* **43**, 8226–8239 (2014).
6. Zaera, F. Molecular approaches to heterogeneous catalysis. *Coord Chem Rev* **448**, 214179 (2021).
7. Barrabés, N. *et al.* Doped metal clusters as bimetallic AuCo nanocatalysts: insights into structural dynamics and correlation with catalytic activity by in situ spectroscopy. *Faraday Discuss* **9**, (2022).
8. Müller, N. *et al.* Dynamic behaviour of platinum and copper dopants in gold nanoclusters supported on ceria catalysts. *Commun Chem* **6**, 1–10 (2023).
9. Sahoo, K., Gazi, T. R., Roy, S. & Chakraborty, I. Nanohybrids of atomically precise metal nanoclusters. *Communications Chemistry 2023 6:1* **6**, 1–14 (2023).
10. Quantum Confinement-Size effects and properties of nanostructures – Nanoscience and Nanotechnology I. https://ebooks.inflibnet.ac.in/msp08/chapter/quantum-confinement-size-effects-and-properties-of-nanostructures/.
11. Geometric and electronic structures of atoms, nanoclusters, and... | Download Scientific Diagram. https://www.researchgate.net/figure/Geometric-and-electronic-structures-of-atoms-nanoclusters-and-nanoparticles-Reproduced_fig1_359867806.
12. Isabel Garcia Yago, C. Thiolate protected gold catalysts for oxidation reactions.
13. Yao, C. *et al.* Mono-cadmium vs Mono-mercury Doping of Au25 Nanoclusters. *J Am Chem Soc* **137**, 15350–15353 (2015).
14. Kang, X., Chong, H. & Zhu, M. Au25(SR)18: The captain of the great nanocluster ship. *Nanoscale* **10**, 10758–10834 (2018).

15. Yamazoe, S., Kurashige, W., Nobusada, K., Negishi, Y. & Tsukuda, T. Preferential location of coinage metal dopants (M = Ag or Cu) in [Au25- xMx(SC2H4Ph)18]- (x ∼ 1) as determined by extended X-ray absorption fine structure and density functional theory calculations. *Journal of Physical Chemistry C* **118**, 25284–25290 (2014).

16. Garcia, C. *et al.* Dynamics of Pd Dopant Atoms inside Au Nanoclusters during Catalytic CO Oxidation. *J. Phys. Chem. C* **124**, 23626–23636 (2020).

17. Truttmann, V. *et al.* CeO2 Supported Gold Nanocluster Catalysts for CO Oxidation: Surface Evolution Influenced by the Ligand Shell. *ChemCatChem* **14**, e202200322 (2022).

18. CHAPTER 1: LITERATURE REVIEW N. Ntholeng Chapter 1 Literature Review.

19. Castro-Latorre, P., Neyman, K. M. & Bruix, A. Systematic Characterization of Electronic Metal-Support Interactions in Ceria-Supported Pt Particles. *Journal of Physical Chemistry C* **127**, 17700–17710 (2023).

20. Beniya, A. *et al.* CO oxidation activity of non-reducible oxide-supported mass-selected few-atom Pt single-clusters. *Nature Communications 2020 11:1* **11**, 1–10 (2020).

21. Li, Y. *et al.* Interface Engineering of Gold Nanoclusters for CO Oxidation Catalysis. *ACS Appl Mater Interfaces* **10**, 29425–29434 (2018).

22. Cai, G. *et al.* Hydrogen production via water-gas shift reaction by Cu/SiO2catalyst: A case study of CeO2doping. *Energy and Fuels* **35**, 3521–3528 (2021).

23. Lavenn, C., Demessence, A. & Tuel, A. Au25(SPh-pNH2)17 nanoclusters deposited on SBA-15 as catalysts for aerobic benzyl alcohol oxidation. *J Catal* **322**, 130–138 (2015).

24. Zhang, B. *et al.* Ligand Migration from Cluster to Support: A Crucial Factor for Catalysis by Thiolate-protected Gold Clusters. *ChemCatChem* **10**, 5372 (2018).

25. Truttmann, V. *et al.* Structural evolution after oxidative pretreatment and CO oxidation of Au nanoclusters with different ligand shell composition: a view on the Au core. *Physical Chemistry Chemical Physics* **25**, 3622–3628 (2023).

26. Pollitt, S. *et al.* The Dynamic Structure of Au38(SR)24Nanoclusters Supported on CeO2upon Pretreatment and CO Oxidation. *ACS Catal* **10**, 6144–6148 (2020).

27. Banu, R. *et al.* Synergistic effect of ligand-cluster structure and support in gold nanocluster catalysts for selective hydrogenation of alkynes. *Nanoscale* **17**, 5098–5105 (2025).

28. Timoshenko, J. & Roldan Cuenya, B. In Situ/ Operando Electrocatalyst Characterization by X-ray Absorption Spectroscopy. *Chem Rev* **121**, 882–961 (2021).

29. Schilling, C. & Hess, C. Elucidating the Role of Support Oxygen in the Water-Gas Shift Reaction over Ceria-Supported Gold Catalysts Using Operando Spectroscopy. *ACS Catal* **9**, 1159–1171 (2019).

30. Song, W. & Hensen, E. J. M. Mechanistic aspects of the water-gas shift reaction on isolated and clustered Au atoms on CeO2(110): A density functional theory study. *ACS Catal* **4**, 1885–1892 (2014).

31. Sera, M. *et al.* Atomically Precise Au 24 Pt(thiolate) 12 (dithiolate) 3 Nanoclusters with Excellent Electrocatalytic Hydrogen Evolution Reactivity.

32. Truttmann, V. *et al.* CeO2 Supported Gold Nanocluster Catalysts for CO Oxidation: Surface Evolution Influenced by the Ligand Shell. *ChemCatChem* **14**, e202200322 (2022).

33. Tesvara, C. *et al.* Unraveling the CO Oxidation Mechanism over Highly Dispersed Pt Single Atom on Anatase TiO2 (101). *ACS Catalysis* **14**, 7562–7575 (2024).

34. Doherty, R. P. *et al.* On the promoting effect of Au on CO oxidation kinetics of Au–Pt bimetallic nanoparticles supported on SiO2: An electronic effect? *J Catal* **287**, 102–113 (2012).

35. Bosio, N., Di, M., Skoglundh, M., Carlsson, P. A. & Grönbeck, H. Interface Reactions Dominate Low-Temperature CO Oxidation Activity over Pt/CeO2. *Journal of Physical Chemistry C* **126**, 16164–16171 (2022).

36. Smith R J, B., Loganathan, M. & Shantha, M. S. A review of the water gas shift reaction kinetics. *International Journal of Chemical Reactor Engineering* **8**, (2010).

37. Fu, Q., Kudriavtseva, S., Saltsburg, H. & Flytzani-Stephanopoulos, M. Gold–ceria catalysts for low-temperature water-gas shift reaction. *Chemical Engineering Journal* **93**, 41–53 (2003).

38. Sera, M. *et al.* Atomically Precise Au24Pt(thiolate)12(dithiolate)3 Nanoclusters with Excellent Electrocatalytic Hydrogen Evolution Reactivity. *J Am Chem Soc* **146**, 29684–29693 (2024).

39. Method synthesizin TBBT TDT cluster out of PET. https://pubs.acs.org/doi/suppl/10.1021/jacs.4c10868/suppl_file/ja4c10868_si_001.pdf.

40. Fornasini, P. Lecture Notes on Extended X-ray Absorption Fine Structure (EXAFS). (2023).

41. EXAFS - Theory - Chemistry LibreTexts. https://chem.libretexts.org/Bookshelves/Physical_and_Theoretical_Chemistry_Textbook_Maps/Supplemental_Modules_(Physical_and_Theoretical_Chemistry)/Spectroscopy/X-ray_Spectroscopy/EXAFS_-_Theory.

42. Ravel, B. & Kelly, S. D. The Difficult Chore of Measuring Coordination by EXAFS.

43. Prajapati, A. *et al.* Best practices for in-situ and operando techniques within electrocatalytic systems. *Nature Communications 2025 16:1* **16**, 1–20 (2025).

44. Chen, L. *et al.* Advances in in situ/operando techniques for catalysis research: enhancing insights and discoveries. *Surface Science and Technology 2024 2:1* **2**, 1–23 (2024).

45. Ravel, B. & Newville, M. ATHENA, ARTEMIS, HEPHAESTUS: data analysis for X-ray absorption spectroscopy using IFEFFIT. *urn:issn:0909-0495* **12**, 537–541 (2005).

46. Rehr, J. J. *et al.* Ab initio theory and calculations of X-ray spectra. *C R Phys* **10**, 548–559 (2009).

47. Yang, D. *et al.* Controllable Conversion of CO2 on Non-Metallic Gold Clusters. *Angewandte Chemie - International Edition* **59**, 1919–1924 (2020).

48. Sera, M. *et al.* Atomically Precise Au24Pt(thiolate)12(dithiolate)3 Nanoclusters with Excellent Electrocatalytic Hydrogen Evolution Reactivity. *J Am Chem Soc* **146**, (2024).

49. Wan, X. K., Wang, J. Q., Nan, Z. A. & Wang, Q. M. Ligand effects in catalysis by atomically precise gold nanoclusters. *Sci Adv* **3**, (2017).

50. Lan, T. *et al.* Polyoxometalates-Mediated Selectivity in Pt Single-Atoms on Ceria for Environmental Catalysis. *Angewandte Chemie - International Edition* **64**, e202415786 (2025).

51. Qi, Z., Chen, L., Zhang, S., Su, J. & Somorjai, G. A. Mechanism of Methanol Decomposition over Single-Site Pt1/CeO2Catalyst: A DRIFTS Study. *J Am Chem Soc* **143**, 60–64 (2021).

52. Vecchietti, J. *et al.* Shape-Controlled Pathways in the Hydrogen Production from Ethanol Steam Reforming over Ceria Nanoparticles. *ACS Catal* **12**, 10482–10498 (2022).

53. Finelli, V., Rojas-Buzo, S., Signorile, M., Bonino, F. & Bordiga, S. Exploring Ce(IV)-MOFs redox behavior for catalysis by spectroscopies. *Nano materials science* (2024) doi:10.1016/j.nanoms.2024.11.001.

7 Index

7.1 Equations

7.2 Tables

7.3 Figures